Engineering Structures 101 (2015) 477–493

Contents lists available at ScienceDirect

Engineering Structures

journal homepage: www.elsevier.com/locate/engstruct

Monolithic reinforced concrete bridge joints under cyclic excitation

D. Timosidis [a], K.G. Megalooikonomou [b,*], S.J. Pantazopoulou [b,1]

[a] Demokritus University of Thrace (DUTh), Vas. Sofias Street No. 1, Xanthi 67100, Greece
[b] University of Cyprus (UCY), 75 Kallipoleos Street, P.O. Box 20537, 1687 Nicosia, Cyprus

ARTICLE INFO

Article history:
Received 19 December 2014
Revised 31 July 2015
Accepted 3 August 2015

Keywords:
Reinforced concrete bridges
Monolithic connections
Joints
Shear failure
Punching

ABSTRACT

Joint regions in monolithic bridge connections often present geometric complexities owing to the structural detailing of the converging members, such as the occasional presence of passages through the body of the connections, the use of relatively high reinforcing ratios and the type of column section (circular or rectangular). An open issue in such circumstances is the definition of the effective joint area mobilized in shear transfer, and the effectiveness of joint reinforcement placed outside the joint panel in the adjacent members. In order to explore the effects of these geometric complexities with particular reference to the adequacy of the Eurocode 8-II (2005) design guidelines for bridge joints an experimental program was carried out on scaled specimens representing bridge monolithic connections under reversed cyclic loading and combined gravity loads. A total of ten specimens were tested. Of those, six represented pier column-superstructure joints, loaded either in the direction transverse to the bridge axis (four specimens) or along the bridge axis (two specimens), at a scale of 1/5. The remaining four specimens represented column-footing connections at a scale of 1/10. Parameters of study were the presence of openings longitudinally or transversally through the joint, the option of decongesting the joint by placing some of the required reinforcement in the adjacent converging members, the shape of the column cross section and the depth of the connection body since these parameters both define the joint volume engaged in shear transfer. The paper summarizes the experimental programme, the primary findings and the implications on established design practice for improved redundancy of force transfer.

1. Introduction

Design procedures for bridge monolithic connections as a separate class of elements with special performance requirements was introduced for the first time in Eurocode 8-II (EC8-II, 2005) [1]. After the 1989 Loma Prietta earthquake many examples of bridge infrastructure damages were reported, some failures concerning inadequately confined monolithic connections (joints) between pier and superstructure or between pier and caissons [2]. Several experimental programs on monolithic bridge joints under simulated earthquake loading followed, on a variety of specimen forms, specimen scales and loading patterns.

Based on these experimental programs a total of 56 experiments are available in the literature that document performance of bridge monolithic connections under seismic action. Although the number of conducted experiments is low as compared to the sheer variety of existing geometric characteristics and configurations of the joints, a wide range of design parameter combinations have been explored that are known to affect the seismic behavior of joints. These include the geometry of the joint (Sritharan et al. [11], Naito et al. [12], Gibson et al. [14]), the scale of the specimens (Priestley et al. [6]), the design philosophy used in reinforcement detailing (Pantelides et al. [13], Mazzoni and Moehle [10]), the condition of the specimen (prototype, repaired or retrofitted) (Thewalt and Stojadinovic [3], Xiao et al. [4], Sexsmith et al. [5], Lowes and Moehle [8]) and the magnitude of shear stress demand with reference to the capacity. The morphology of the connection has also been a subject of investigation: many specimens represented joints of outrigger beams with columns (Ingham et al. [7]), whereas very few specimens model deck to pier connections or connections between bridge pier and footing (McLean and Marsh [9]). Due to the large variety in specimen form, the number of experiments that are directly comparable among the available tests so as to illustrate the influence of any single variable is still very low. Thus, statistical evaluation of test results and generalization of design methods cannot be drawn.

* Corresponding author at: Department of Civil and Environmental Engineering, School of Engineering, University of Cyprus, 75 Kallipoleos Street, P.O. Box 20537, 1678 Nicosia, Cyprus. Tel.: +357 2289 2221; fax: +357 2289 5080.
E-mail addresses: dtimosid@civil.duth.gr (D. Timosidis), kmegal01@ucy.ac.cy (K.G. Megalooikonomou), pantaz@ucy.ac.cy (S.J. Pantazopoulou).
[1] On leave of absence from DUTh.

http://dx.doi.org/10.1016/j.engstruct.2015.08.004
0141-0296/

Nevertheless, due to the pressing need for design procedures for this problem, the primary outcomes of this research activity served as the basis in drafting the seismic provisions for monolithic connections in the Caltrans [15] and EC8-II [1] design codes. Requirements concern cap-beam to pier connections, beam to pier connections as well as footing to pier connections. The salient points of these design approaches are as follows: (a) A bridge monolithic joint is capacity-designed in shear so as to resist the forces from the adjacent plastic hinge in the pier in the plane of seismic action. (b) The acceptance criteria refer to average joint shear stress, where the peak value of total shear stresses developed at the midpoint of the joint panel is compared against a semi-empirical design value obtained from first principles and calibrated against experimental data [15]. (c) Concrete and reinforcement contributions are separately taken into account in force equilibrium. (d) If the joint shear stress exceeds the limit value associated with concrete cracking, the required joint reinforcement is estimated from force equilibrium; otherwise, minimum joint reinforcement is placed in the joint. (e) Both codes allow the placement of a part of the vertical joint reinforcement in the beam outside of the joint. Although a primary outcome of the experimental research was that anchorage conditions of pier longitudinal reinforcement within the joint is a critical parameter in the assessment of existing joints, Caltrans [15] allows the configuration of straight column anchorages inside joint areas, whereas EC8-II [1] requires formation of hooks at the bar ends near the free joint face.

In particular the EC8-II [1] design provisions were based on an extension of a mechanistic model originally developed from building joints. To-date, these provisions have not been tested against experiments that represent the special morphology of bridge connections. To assess several of the open issues in the adopted design requirements and recommendations (such as the bond conditions of the main pier reinforcement anchorages, the effective joint area, the presence of openings in the body of the joint panel) with particular reference to the effectiveness of the Eurocode 8-II (2005) [1] design guidelines for bridge monolithic connections an experimental program was carried out on bridge joint specimens under reversed cyclic loading that simulates earthquake effects, along with combined axial loads. The following section provides a brief review of the current seismic design provisions in the European practice which serves as a background to the problem studied; the experimental program is presented in detail in the subsequent chapters of the paper.

2. Design background on bridge monolithic connections

For the benefit of better appreciation of the open issues in detailing and dimensioning bridge joints the following sections present a brief review of the relevant seismic design requirements currently in force in the European practice. Forces are associated to the formation of a plastic hinge in the bridge pier adjacent to its connection either at the top (to the cap-beam) or at the bottom (to the footing or pile-cap). Calculations refer to the center of the joint where moment transfer is evaluated as depicted in Fig. 1.

2.1. Summary of EC8-II (2005) requirements for bridge joint verification

In the EC8-II [1] requirements and guidelines for the design of bridge column-to-cap beam or superstructure joints reference is made to a solid joint panel, therefore certain bridge-specific details (openings, members with box-cross sections) are not actually addressed. A column with a solid rectangular cross section of section height h_c and width b_c (perpendicular to the plane in which the joint is studied) is considered. For the purpose of stress reduction from stress resultants the effective width of the joint $b_{j,eff}$ of the joint is defined as follows:

(a) When the column frames into a slab or into a transverse rib of a hollow slab:

$$b_{j,eff} = b_c + 0.5 \cdot h_c \tag{1}$$

(b) When the column frames directly on a longitudinal web of width b_w (where b_w is parallel to b_c):

$$b_{j,eff} = \min\{b_w, b_c + 0.5 \cdot h_c\} \tag{2}$$

(c) For circular column of diameter d_c, the above definitions are still applicable taking:

$$b_c = h_c = 0.9 \cdot d_c \tag{3}$$

(thus the design provision do not distinguish between a rectangular and a circular column section shape in determining the effective joint dimensions). Joint demand in terms of forces transferred through the joint and the corresponding joint stress are obtained by considering the free body diagram of the left (or right) part of the joint panel after a vertical section through the joint. With reference to Fig. 1, the design vertical shear force, V_{jz}, transferred through the joint is equal to:

$$V_{jz} = T_c - V_{br} = \alpha \cdot f_y \cdot \frac{A_{s,col}}{2} - V_{br} \tag{4}$$

where $T_c = 0.5 \cdot A_{s,col} \cdot f_y$ is the resultant force of the tensile reinforcement of the column that is associated with the design flexural resistance M_{Rd} of the plastic hinge, α is the over-strength factor and V_{br} is the shear force of the beam adjacent to the tensile face of the column, resulting from capacity-design considerations when a plastic hinge occurs in the column (Fig. 1).

The design horizontal shear of the joint V_{jx} is evaluated from the following equation:

$$V_{jx} \cdot z_b = V_{jz} \cdot z_c \tag{5}$$

where $z_b = 0.9 \cdot h_b$ is the internal force lever arm of the beam's section at the face of the joint and $z_c = 0.9 \cdot h_c$ is the internal force lever arm of the column's section within the plastic hinge location at the face of the joint.

Joint shear strength verification is carried out at the joint center, where in addition to V_{jz} and V_{jx}, the simultaneous influence of the following axial forces is taken into account:

(a) The vertical axial joint force N_{jz} that arises if it is considered that: (i) the gravity related axial stress is uniformly distributed over a horizontal column cross section in the joint region. (ii) Vertical loads are transferred gradually from the deck to the column over the height of a joint. It is assumed that the axial force at the joint-midheight is equal to half of the axial force of the column for T-shaped or Γ-shaped joints when $b_{j,eff} = b_c$. (iii) When $b_{j,eff} > b_c$ the axial force of the joint is reduced following the pattern of stresses which are assumed to be distributed over an effective area that is greater than the area of the column's section. Therefore:

$$N_{jz} = 0.5 \cdot N_{c,G} \cdot \frac{A_c}{A_{j,eff}} = 0.5 \cdot \frac{b_c}{b_{j,eff}} \cdot N_{c,G} \tag{6}$$

where $N_{c,G}$ is the axial force of the column under permanent actions (serviceability limit state).

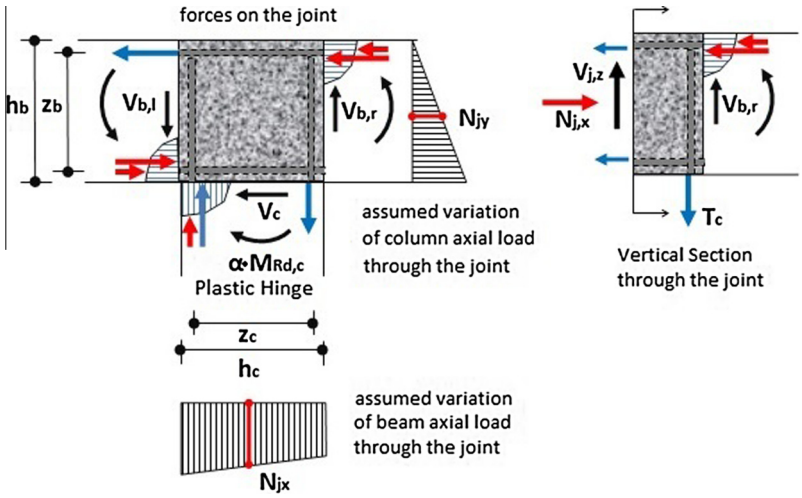

Fig. 1. Joint equilibrium in a bridge monolithic T-connection. (a) Definition of terms. (b) Calculation of joint shear force V_{jz} according with Eq. (4).

(b) The horizontal force N_{jx} is taken equal to the capacity design axial force effects in the beam, including the effects of longitudinal pre-stressing after all losses, if such axial forces are actually effective throughout the width $b_{j,eff}$ of the joint.
(c) A horizontal force N_{jy} in the transverse direction is considered if pre-stressing is present; it is taken equal to the effect of transverse pre-stressing after all losses and it is assumed to be effective within the height h_c of the column's cross section.

Details of the mechanics background to the recommended procedures for joint stress verification as per EC8-II [1] are provided in the Appendix. The provisions are intended to preclude formation of plastic hinging within the body of the joint and they apply to any type of connection including joints between bridge piers and caissons under the design seismic action. In the case of pile-cap foundation it is usually difficult to avoid local plastification of the piles due to the large difference in stiffness between the connecting members. In such cases the integrity and the ductile behavior of the piles should be secured through proper detailing. EC8-II [1] considers the connections between bridge piers and caissons in the same way as it addresses the monolithic connections between pier and superstructure. It requires that the joints between vertical ductile columns and foundations, next to the location of the plastic hinge, should be designed with capacity design considerations in the direction under study. The requirements described already for the connections between pier and cap-beam are valid also for the design of joints between bridge piers and caissons. Here the role of the cap-beam is substituted by the body of the footing.

2.2. Open issues in the design practice of bridge monolithic connections

Despite recent progress marked by the introduction of design rules as outlined in the preceding, some issues are still open with regards performance and design of monolithic connections under seismic force transfer. For one, the bond conditions of the main pier reinforcement anchorages are not explicitly taken into account in these requirements, even when large diameter bars are used [16]. The empirical requirement by EC8-II [1] that a hook should be provided at the end of anchorages is the only code requirement towards this objective. A most critical open issue is definition of the effective joint area, through which the shear stress demand is calculated from the joint forces. This concern is particularly encountered when dealing with monolithic connections between framing members with hollow sections or box girders that commonly occur in bridge bents [17]. Actually, very few experimental data exist in the literature regarding monolithic RC bridge joints where the superstructure is composed by box-shaped girders. Another characteristic that has not been studied so far is the presence of openings in the body of the joint panel; these openings are traditionally used as passages for inspection of the box-shaped girders framing into the joints. This is a bridge-specific geometric detail that commonly occurs in European design practice and which is not addressed by the recent codes. Clearly, direct extension of design code requirements for beam-column connections that had been originally derived for buildings cannot be simply transferred to monolithic connections of bridge structures by transposing the location of the plastic hinge from the beam to the pier. The open issues outlined are the motivating objectives of the experimental study presented in detail the remainder of this paper. The experimental findings are used for the evaluation of the design model and requirements of EC8-II [1] for bridge monolithic joints.

3. Experimental program

A total of ten connection specimens modeling various arrangements of bridge monolithic joints were tested in the experimental program presented in this paper. Six of the specimens represented joints between pier and superstructure, built at a scale of 1/5, whereas the remaining four specimens were designed to represent connections between bridge piers and caissons at a 1/10 scale. All specimens were tested under simulated earthquake loading. The objective of the study was to investigate the performance of monolithic RC bridge connections providing insight as to the effective joint area that is mobilized in shear and moment transfer in the connection, particularly in the case of geometric details that are specific to bridges such as the presence of openings through the joint body as well as connections between box-sectioned members. Observing the prevailing modes of failure in such circumstances is an important aspect of the experimental investigation that may be used to enrich and complete the relevant provisions. Another aspect of investigation is the configuration and layout of steel reinforcement inside the joint panel including the pattern of pier column bar anchorages into the adjacent beams of the superstructure or footings.

3.1. Specimen design

The prototypes that were used in this study in order to determine the details of the specimens were monolithic concrete bridges located along the Egnatia highway [18] in Greece. Six of the specimens (A1–A6, Group A specimens) were designed to represent single column-to-superstructure connections. Four connection specimens (A1–A4) modeled at 1/5 scale the geometry and actions occurring in connections swaying in the direction perpendicular to the bridge axis (Fig. 2a and b) whereas the remaining two specimens (A5 and A6) modeled connections swaying in the direction parallel to the bridge axis (Fig. 2c). In the remainder of this presentation these are denoted as group A specimens (A1–A6). All connections comprised a T-joint, but joint geometry and reinforcement arrangement were parameters of investigation (Fig. 3). The main characteristics of the joints of group A specimens are reported in Table 1. Specimen A1 was designed and detailed according with EN1998-2 [1] (Fig. 3, see Appendix B). Specimen A2 was designed with the same geometry as A1, but with part of the required joint reinforcement placed in the primary beams adjacent to the joint. This alternative placement of joint shear reinforcement is allowed in EC8-II [1] and CALTRANS [15] so as to avoid reinforcement congestion (Fig. 3). Specimen A3 was designed with the same dimensions as A1, but with an inspection opening in the joint body in order to evaluate this construction practice in bridge monolithic joint connections (Fig. 3). Specimen A4 was designed with reduced cap beam width, in order to check whether the increased width for cap beams required by EC8-II [1] is indeed an essential requirement (Fig. 3). Specimen A5 was designed also according with EC8-II [1], but it was tested for force

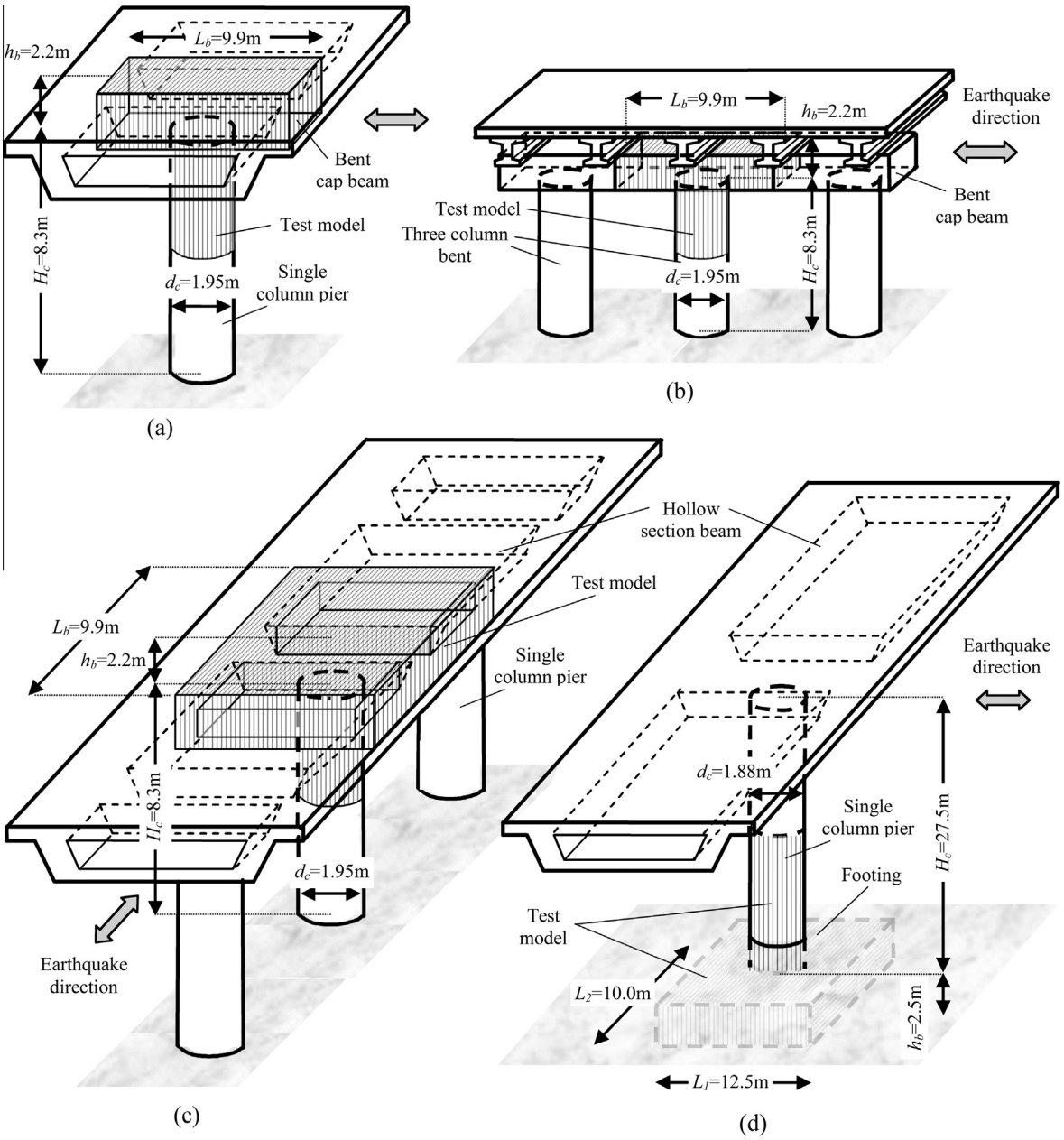

Fig. 2. Representation of the prototype bridge structure commonly encountered in Egnatia avenue and the test model for: (a and b) A1–A4 specimens, (c) A5 and A6 specimens and (d) B1–B4 specimens. Fig. 2a and b represent the circumstances modeled by all specimens A1–A4. Fig. 2c represents specimens A5 and A6. Fig. 2d refers to all specimens of type B.

and moment transfer acting in the direction of the bridge axis. This is the first reported beam-to-column specimen designed with a hollow section of beam (Fig. 3). Moreover it has an opening for inspector passage in the joint panel (as in the case of specimen A3), in order to evaluate the influence of the openings when force transfer occurs in the longitudinal bridge axis (Fig. 3). Specimen A6 was designed with the same dimensions as A5, but without the opening for inspector passage in the joint panel.

The remaining four specimens (B1–B4, Group B specimens) represented connections between single column-pier and footing and were conducted at a smaller scale due to restrictions of the testing equipment (Fig. 2d). Parameters of study in the case of group B specimens were the shape of the column cross section (circular vs. rectangular) and the height of the joint (which here is identical with the footing height) (Fig. 4). The main characteristics of the joints of group B specimens are reported in Table 2. Specimen B1 was designed with a circular column cross-section and a conventional footing height, with joint reinforcement arranged according with EC8-II [1] (Fig. 4, see Appendix C). Specimen B2 was designed as with B1, but with a reduced footing height, in order to establish whether the height required by EC8-II [1] is an essential requirement or whether it can be relaxed (Fig. 4). Specimen B3 was designed as B1, but with a rectangular column section (Fig. 4). Specimen B4 was designed as B3, but with a reduced footing height (Fig. 4). A detailed description of all specimens is given in Timosidis 2009 [18].

All steel reinforcements used for the construction of the specimens were EC2 (2004) compliant C500 deformed bars [19], with a nominal yield strength of $f_y = 500$ MPa, ratio of maximum strength to yield strength between 1.15 and 1.35 ($1.15 \leqslant f_u/f_y \leqslant 1.35$) and tension strain ductility at failure in excess of 7.5 ($\varepsilon_u/\varepsilon_y \geqslant 7.5$). Concrete material properties were determined from standard compression tests of 150×300 mm concrete cylinders that had been cast and cured along with the test specimens (Table 3, average values at time of component testing).

3.2. Experimental setup

Specimens of Group A were placed in the reaction frame rotated at 90° with respect to the vertical axis as shown in Fig. 5. The specimen carried moment transfer through pinned supports at the strong floor and at the cap beam of the reaction frame. Group B specimens were placed in a smaller capacity reaction frame in the normal position as shown in Fig. 6. During the tests the column footing was wedged inside a concrete block where frictional contact and lateral bearing developed at the interface. The concrete block encased the specimen footing in order to prevent specimen sliding in the plane of action while allowing for vertical bearing and uplift as in common footings. All specimens were initially subjected to loads that were simulating gravity load effects; these loads were applied through stressing of four high strength rods through two spreader beams placed at the ends of the columns that straddled the specimens. The reacting point loads produced shears and moments either in the beams at the joint faces (group A specimens) or in the footings at the joint faces (group B specimens) and an axial force in the columns, equal to the scaled values which would be expected in the prototype connections due to gravity loads. Thus, the applied column axial load was equal to $N_c = 0.02A_g f_{cm}$ for group A specimens and $N_c = 0.113A_g f_{cm}$ or $N_c = 0.118A_g f_{cm}$ for B1 and B2 or B3 and B4 specimens, respectively (A_g is the gross section of the column and f_{cm} is the mean concrete compressive strength).

Lateral load reversals simulating earthquake effects were applied to the connection upon complete application of the gravity loads, acting quasi-statically at the end of the column through an idealized pin. Especially for the A specimens the cyclic force acted transversally to the longitudinal axis of the column and was applied using two hydraulic actuators for the two directions of loading, respectively. The applied displacement history is given in Fig. 7, given in multiples of the yield displacement which was determined experimentally during the test. Loading up to column yielding was carried out using load control; application was reverted to displacement control beyond that point. Three cycles were performed at each loading step to $0.50F_y$, $0.75F_y$ and $1.00F_y$, where F_y is the estimated load for column yielding of the specimen obtained from flexural analysis of the critical section. (The procedure that has been followed in order to define F_y is through the bi-linearization process of the flexural force–displacement response envelope). Beyond column yielding, lateral loading was applied under displacement control. Three cycles were performed at each loading step to $1.5\Delta_y$, $2\Delta_y$, $4\Delta_y$ and $6\Delta_y$, where Δ_y was the recorded lateral displacement of the column end at the first cycle of the loading step to $1.00F_y$ (Fig. 7). Larger displacements (to ductilities higher than 6) were not applied even for the specimens that could resist them, because of the termination of the actuators' travel.

In the case of B specimens the column gravity loading was large enough to prevent rocking of the specimens at the base. Lateral load reversals were transferred to the supporting concrete block through friction, using the same displacement history as in the case of A specimens except that (a) the force-controlled steps before yielding of the specimens were performed only to $0.50F_y$ and $1.00F_y$ and (b) only one cycle was performed for the displacement-controlled step of $1.5\Delta_y$ (Fig. 7).

During testing, the column axial load was mechanically controlled to its initial value. Three categories of measurements were taken during each test: forces, displacements and strains. Column axial force and lateral applied force were recorded through load cells. Linear variable displacement transducers were used to monitor specimen translations and joint distortions. For group B specimens, analog displacement transducers were also used to measure the footing uplift due to simulated earthquake loads. Strain gauges were used to record the strains developed in the joint transverse reinforcement (at transverse bars located at the joint–column interface and at the joint mid-height). In the case of some specimens strain gauges were also attached along the anchorages of the extreme column main bars to record the strain distribution along the anchorages. In addition, digital images of the entire specimen and of the joint surface were used to monitor deformations (strains) at each loading point by stable cameras. Variations in the geometry of an array of targets placed in the joint region and in the plastic hinges were used to resolve surface strains and to calculate principal values and orientations (as in the case of strain rosettes).

Using the experimentally recorded data the resistance curve (lateral load vs. lateral displacement) and joint shear stress vs. joint shear distortion for each subassembly were established. Lateral displacement values at the column end were corrected at each loading point by subtracting the displacement components due to the rotation of the testing frame (for group A specimens) or due to the uplift of the footing (for group B specimens); load–displacement envelopes are plotted in Fig. 8 for all specimens.

Joint shear stresses were obtained at each loading point from the free body diagram of the specimen and from force equilibrium of the joint body according with the detailed provisions of EC8-II [1] as summarized in Appendix A. Joint distortion was calculated from the measurements of the two differential transducers (DT's) along the diagonals of the joint face or from the measurement of the same distances on the digital crops according with geometric compatibility as given in Eq. (7):

$$\gamma_{exp} = \tan^{-1}(X/Y) - \tan^{-1}((X + \Delta X)/(Y + \Delta Y)) \quad (7)$$

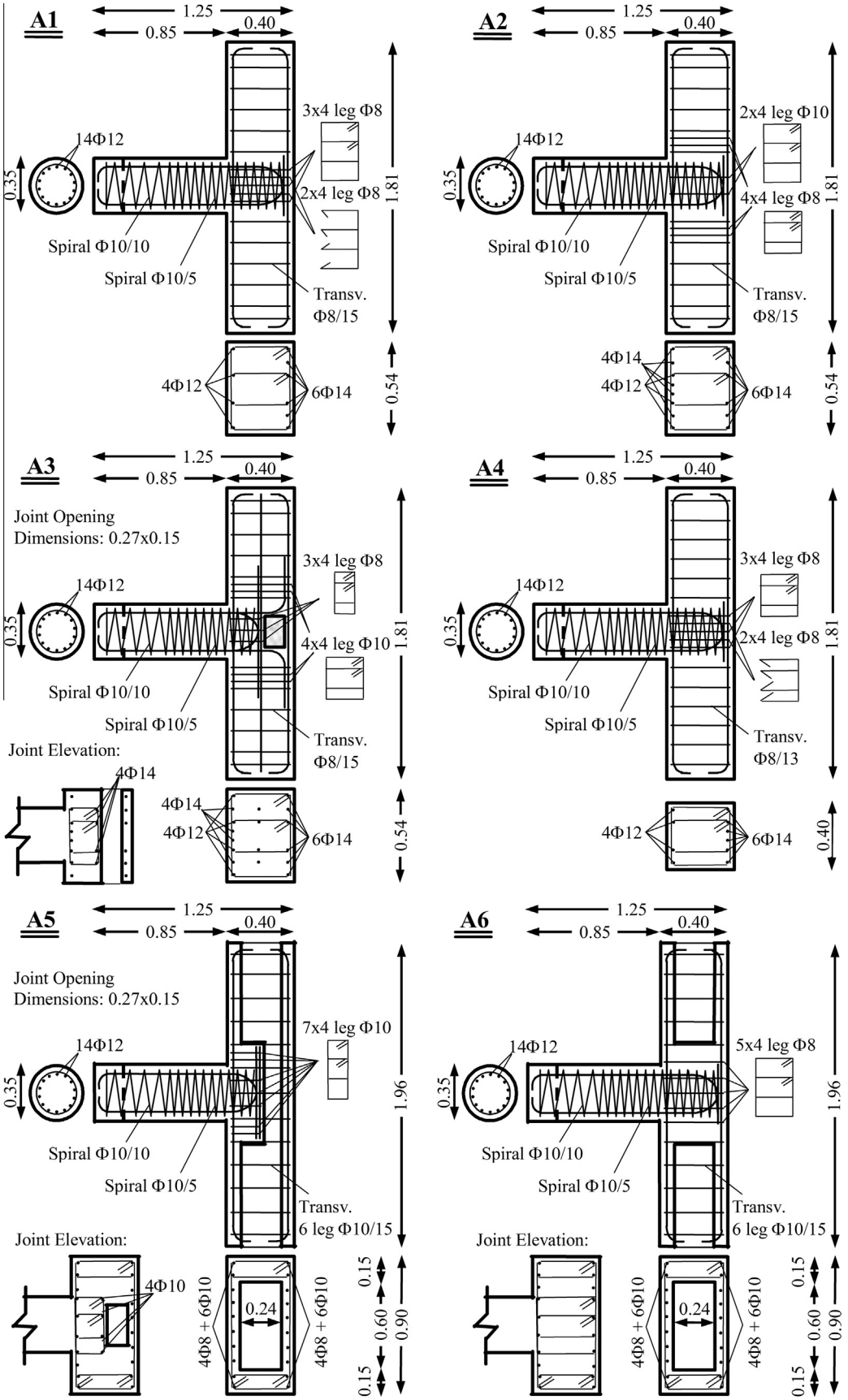

Fig. 3. Geometry and reinforcement arrangement for Group A specimens.

Table 1
Characteristics of the joints of Group A specimens.

Characteristics of the joints of specimens A1–A6						
Specimen	A1	A2	A3	A4	A5	A6
Effective joint dimensions $b_{j,eff} \times h_j$ (m)	0.473 × 0.400	0.473 × 0.400	0.473 × 0.200	0.350 × 0.400	0.473 × 0.400	0.473 × 0.200
Vertical joint shear reinforcement ρ_{jz}	0.68%.	0.42%	0.50%	0.79%	0.68%	0.66%
Horizontal joint shear reinforcement ρ_{jh}	0.94%	0.94%	0.40%	0.91%	0.94%	0.94%

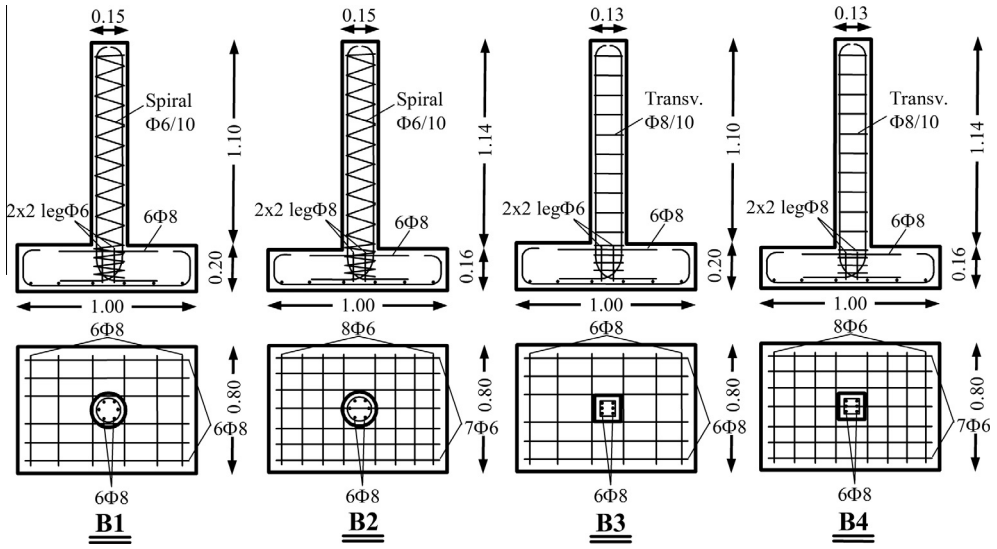

Fig. 4. Geometry and reinforcement arrangement of Group B specimens.

Table 2
Characteristics of the joints of Group B specimens.

Characteristics of the joints of specimens B1–B4				
Specimen	B1	B2	B3	B4
Effective joint dimensions $b_{j,eff} \times h_j$ (m)	0.203 × 0.200	0.203 × 0.160	0.195 × 0.200	0.195 × 0.160
Vertical joint shear reinforcement ρ_{jz}	0.73%	0.73%	0.79%	0.79%
Horizontal joint shear reinforcement ρ_{jh}	0.56%	0.70%	0.58%	0.72%

Table 3
Concrete material properties for all specimens.

Specimen		Days of test	f_{cm} (MPa)	$E_{cm,o}$ (MPa)
A1		176	27.55	9910
A2		251	29.14	12,445
A3		259	29.30	11,725
A4		302	29.85	10,705
A5	Beam	30	26.00	9440
	Column	28	33.95	15,595
A6	Beam	88	26.30	5970
	Column	86	45.00	14,645
B1–B4		120	22.45	10,935

where X was the distance between end points a' and c' of the first diagonal at the joint face, Y was the distance between end points b' and d' of the other diagonal of the joint face, with line (a'–c') being orthogonal to line (b'–d'), and ΔX, ΔY were the length changes of the joint diagonals respectively, with progressive loading (Fig. 9). Furthermore using the DT's mounted adjacent to the column and in the end of the plastic hinge region, the average strain developed in the extreme main column bars inside the plastic hinge length and the pullout slip of the same bars from the joint was also estimated. Note that the joint distortion based on the two DT's along the diagonals of the joint face or from the measurement of the same distances on the digital crops was calculated only for the group A specimens; the experimental envelopes for joint distortion is plotted in Fig. 10 against joint shear stress. The footing face of the group B specimens was too far from the joint area due to its larger thickness; thus measurements on the footing face could not lead to precise estimations of the joint distortion.

4. Discussion of specimen behavior

Fig. 8 plots the response envelope of the lateral displacement versus applied column shear relationship, experimentally obtained for the two groups of specimens. Specimens A1 and B1 serve as control specimens for each one of the two subgroups; because each specimen has some identifying feature that sets it apart from the others, the most important aspects of their behavior are discussed separately in the following sections. The following paragraphs describe the behavior of the test specimens in terms of the observed performance, visible damage, nominal joint strengths and load-deformation relations. Fig. 11 summarizes pictures of the joint region of each specimen of group A at the end of the test, illustrating the observed modes of damage. Complete hysteresis load–displacement curves are plotted in Fig. 12. Similarly, the column footing connection region is illustrated for group B specimens

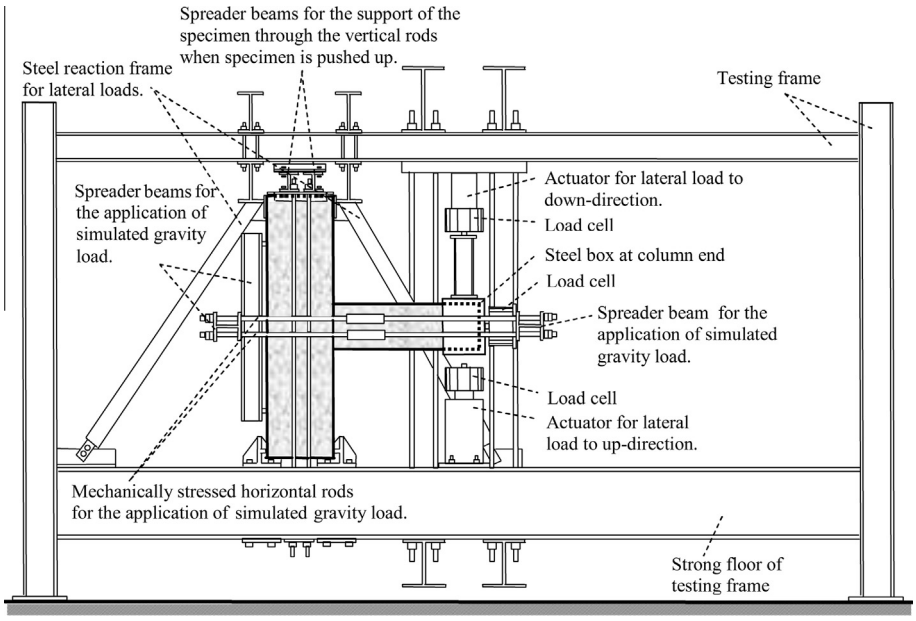

Fig. 5. Test setup for group A specimens.

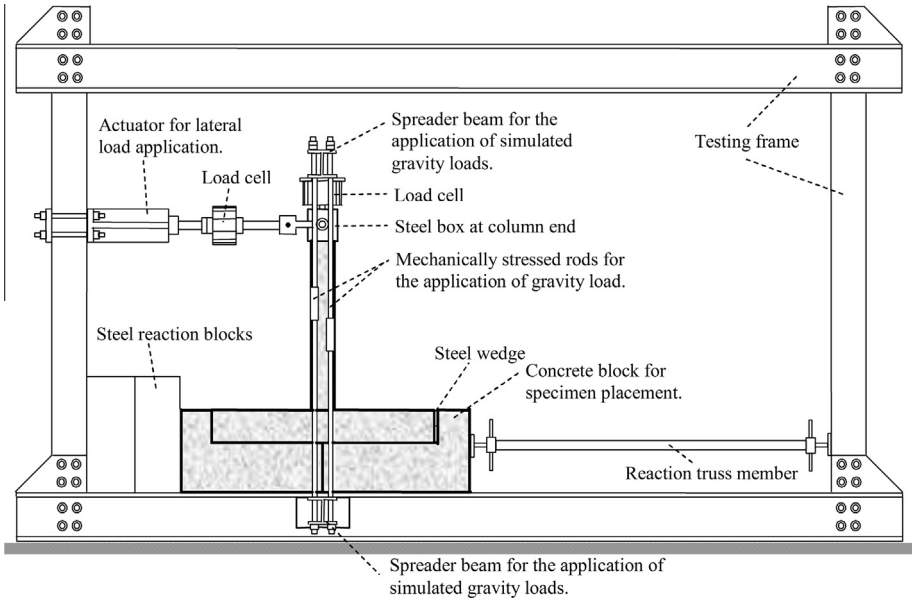

Fig. 6. Test setup for group B specimens.

at the end of the tests in Fig. 13, whereas the hysteresis load–displacement curves for these specimens are given in Fig. 14.

4.1. Control specimen A1

During the force-controlled cycles of the test (cycles $0.50F_y$, $0.75F_y$ and $1.00F_y$), specimen A1 showed only flexural cracks within the column critical length (over a length equal to the column diameter, D, measured from the face of the deck beam soffit). In the following loading steps to $1.50\Delta_y$ and $2.00\Delta_y$, the column flexural cracks propagated and became wider, while minor diagonal shear cracks also appeared at the column faces. The first minor diagonal cracks at the joint faces occurred also at a displacement to $1.50\Delta_y$. Joint diagonal cracks extended at the bottom beam face towards the perimeter of the column, in a radial direction. During the first cycle at $1.50\Delta_y$ the vertical joint shear stress reached the value of $0.38\sqrt{f_{cm}}$ and the joint exceeded yielding as the joint shear stress–joint shear distortion envelope entered the plastic region (Fig. 10) even if it was not clear from external observation. Joint yielding was confirmed by the amount of slip of the extreme column longitudinal reinforcement, which at this stage was 3.0 mm. The maximum attained joint shear stress was equal to $0.49\sqrt{f_{cm}}$ during the first cycle at $\mu_\Delta = 2$. Joint cracks extended only slightly after $\mu_\Delta = 4$, while the flexural column cracks near the joint-column connection became very wide indicating slip at the main column reinforcement anchorage inside the joint (Fig. 11). At the end of the test measured slip of the extreme column longitudinal reinforcement was around 10.0 mm. The overall behavior of the

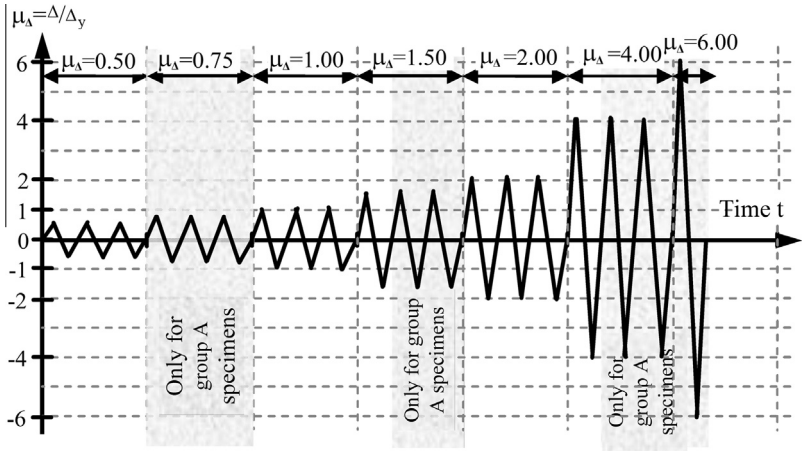

Fig. 7. Lateral loading pattern.

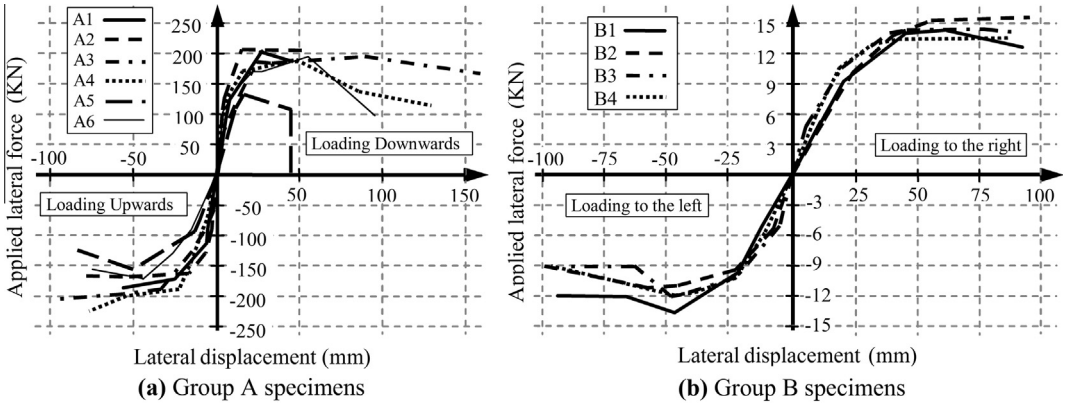

Fig. 8. Response envelope of lateral displacement versus applied load for all specimens.

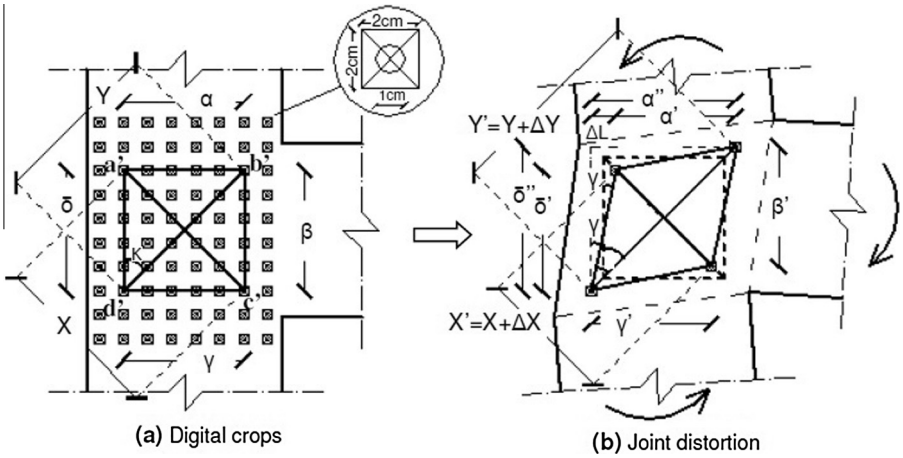

Fig. 9. Measurements for joint distortion.

specimen (Fig. 12) was in conformity with the design philosophy by which it was detailed, with the damage concentrated in the column critical region and the joint entering the plastic response range after the first cycle at $\mu_\Delta = 1.50$, but showing only minor diagonal cracking near the end of the test (i.e., compliance due to damage being overwhelmed by pullout of reinforcement).

4.2. Transverse reinforcement placed outside the joint panel – specimen A2

The behavior of specimen A2 was similar to that of A1 confirming the excellent behavior of the test specimen despite the detailing decision to place some of the required joint reinforcement in

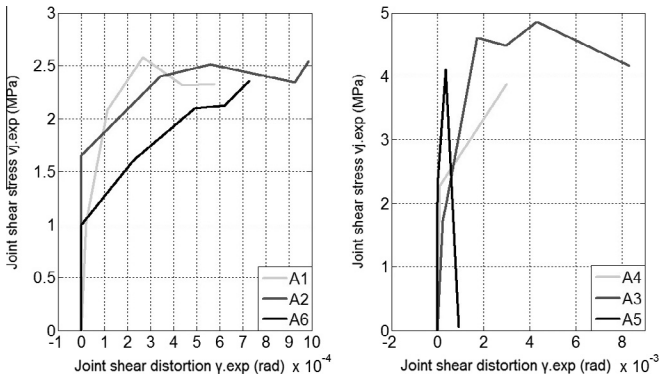

Fig. 10. Response envelope of joint shear stress versus joint distortion for group A specimens.

the adjacent beams. During the force-controlled cycles of the test, A2 showed flexural cracks at the column critical area whereas the first minor shear cracks appeared on the joint faces. At loading steps of $1.50\Delta_y$, the vertical joint shear stress reached the value of $0.29\sqrt{f_{cm}}$ – i.e. exhibiting lower yield strength than A1 (Fig. 10), whereas slip of the extreme column longitudinal reinforcement at this stage was 2.6 mm. The yielding of joint reinforcement was not perceptible other than through propagation of diagonal cracking. As with A1, peak joint shear stress was $0.48\sqrt{f_{cm}}$, attained at a displacement ductility $\mu_\Delta = 2$ and sustained up to $\mu_\Delta = 4$. Cover spalling occurred in the critical column region during the second cycle to a displacement of $2.00\Delta_y$; damage spread further out in the following loading steps. Buckling of column longitudinal reinforcement occurred at $\mu_\Delta = 4$; at that point the test was terminated due to exhaustion of the loading system's travel even though the specimen was still able to sustain its load capacity. The overall behavior (Fig. 12) of the specimen was excellent, conforming to the objectives of the design. As with A1, compliance in the end of the test was overwhelmed by bar pullout slip which was increased to 30.0 mm, while joint cracking, which first occurred at $\mu_\Delta = 1.5$, did not propagate any further.

4.3. The effect of a transverse opening through the body of the joint – specimen A3

Similar to A1 and A2, specimens A3 and A4 both represented connections with a cap beam running in the transverse direction of the frame. Thus, the opening in specimen A3 was intended to model a passage in the longitudinal axis of the bridge. In this case column flexural cracking occurred from the first cycles of loading that continued to propagate from cycle to cycle. Except for the flexural cracks, diagonal shear cracks also formed along the column, which increased in width and severity until the first cycle at $\mu_\Delta = 4.0$. The first shear cracks at the joint faces appeared at the

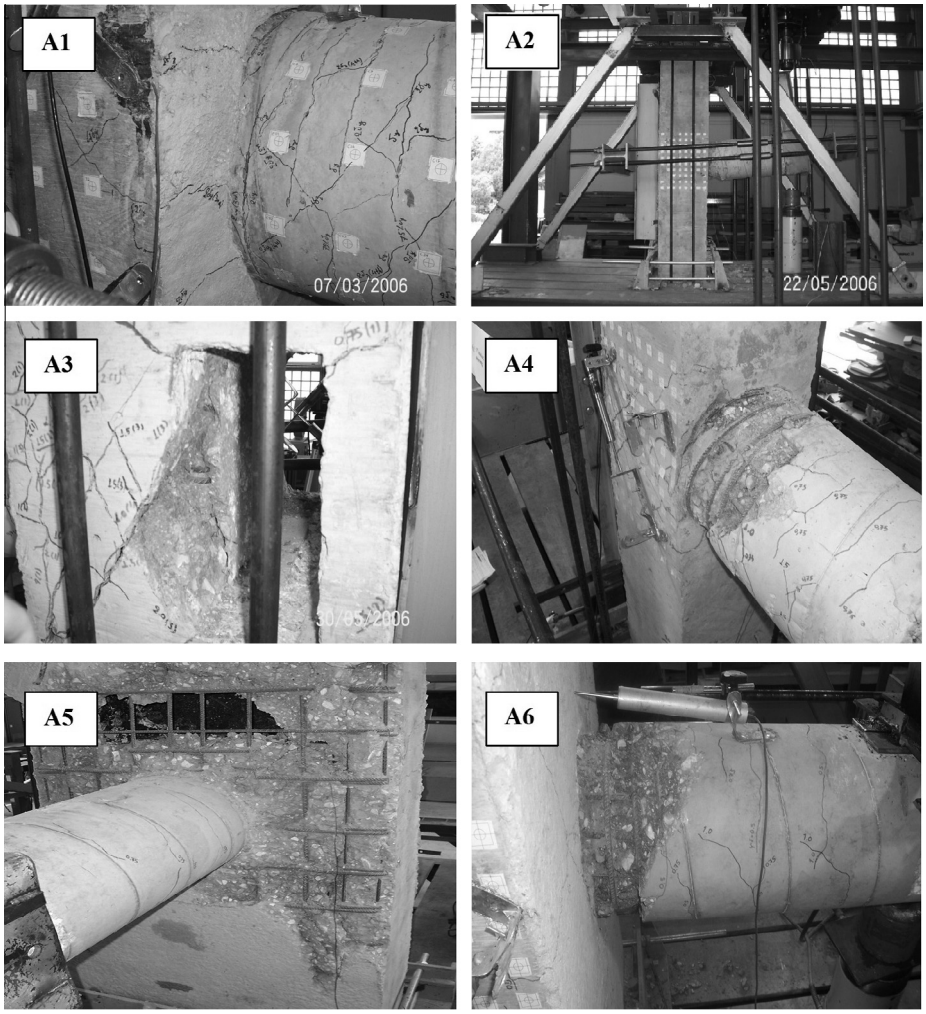

Fig. 11. Failure modes for group A specimens.

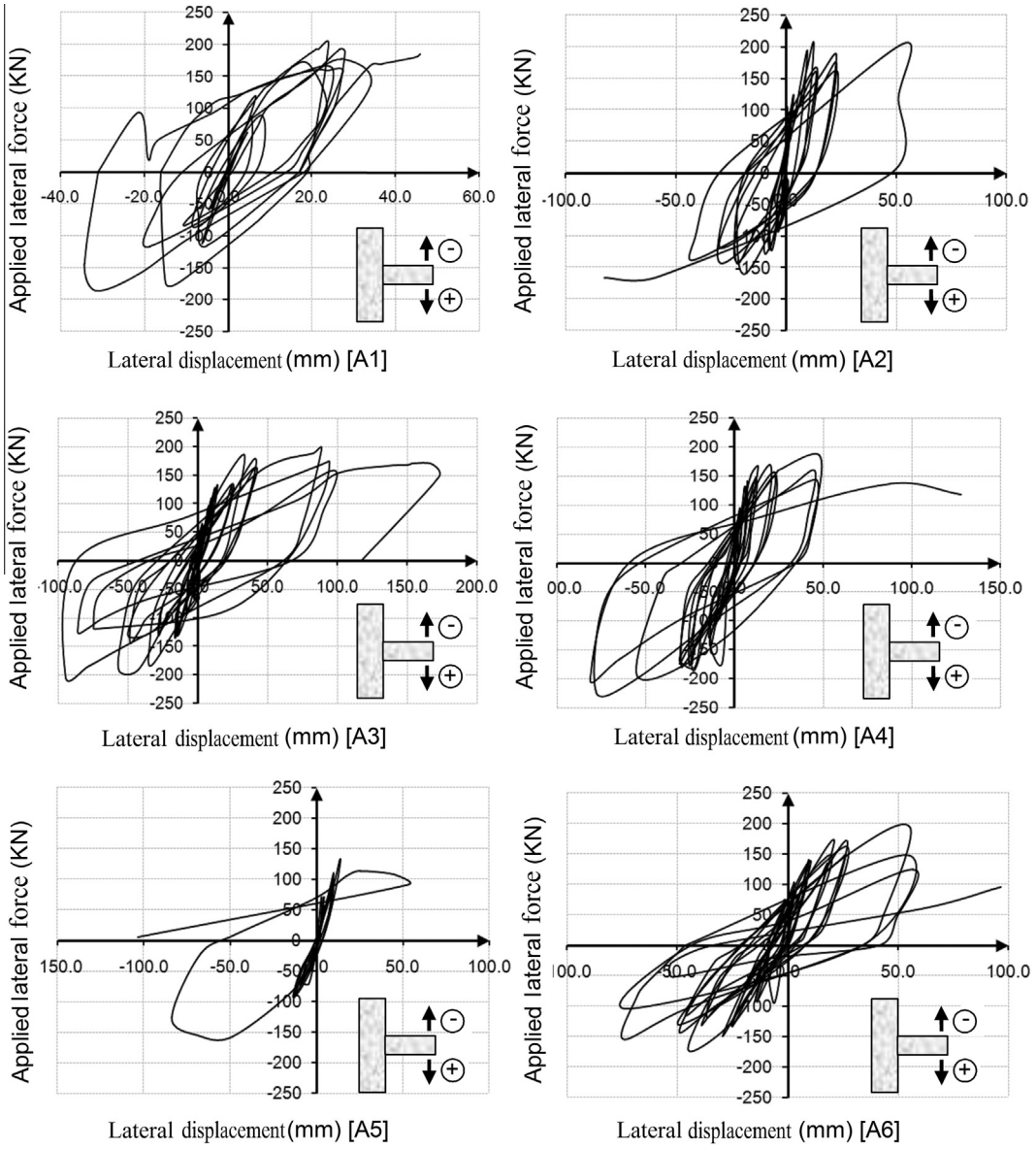

Fig. 12. Cyclic response of column-to-superstructure T-joints.

loading cycle to $0.75F_y$; at the ends of the joint diagonal cracks turned parallel to the longitudinal column reinforcement when the load was increased to $1.00F_y$, indicating large values of anchorage slip. During the post-yielding loading steps to $\mu_\Delta = 1.5$, 2.0 and 4.0 the shear cracks on the joint faces became about 1.0 mm, 1.2 mm and 2.5 mm wide, respectively. In the cycle to $\mu_\Delta = 2.0$ new flexural cracks formed at the top beam face parallel to the edges of the opening, whereas the concrete spalling on the joint faces and at the column critical region both began in the cycle to $\mu_\Delta = 4.0$. Loading even further to $\mu_\Delta = 6.0$ the joint shear cracks (Fig. 11) did not propagate any further, but the column longitudinal reinforcement buckled, leading to reduced load carrying capacity of the specimen. Maximum joint shear stress was estimated equal to $0.63\sqrt{f_{cm}}$ at the point of first joint yielding, but it attained a maximum value of $0.97\sqrt{f_{cm}}$ at $\mu_\Delta = 4.0$. The associated joint distortion was estimated equal to 0.0011 rad and 0.0044 rad, respectively. Joint shear stress and the associated distortion during the test were calculated for the solid part of the joint, underneath the opening. Note that although the specimen had the opening through its joint panel it sustained with adequacy the same loading history as A1 and A2 (Fig. 7), developing column flexural plastic hinging (Fig. 12). It is interesting to note that the joint developed a shear strain that exceeded 0.009 rad in the first and 0.005 rad in the second loading direction. As a matter of fact, the joint developed shear strains about 10 times higher than A1 and A2 (Fig. 10), without losing its capacity, even though it was evident that in the last loading cycles, strength began to degrade. The satisfactory joint response is attributed to the good anchorage conditions of the longitudinal column reinforcement with an adequate hook in the ends. This is also supported by the estimated value of anchorage slip of the extreme column reinforcement which did not exceed the corresponding value attained by specimen A2, i.e. 30.0 mm.

4.4. The effect of a smaller joint area – specimen A4

Specimen A4 had a significantly smaller cap beam width so as to explore the behavior if a smaller joint region is functioning that what is assumed by EC8-II [1]. It is interesting to note that although column plastic hinge actions transferred through the

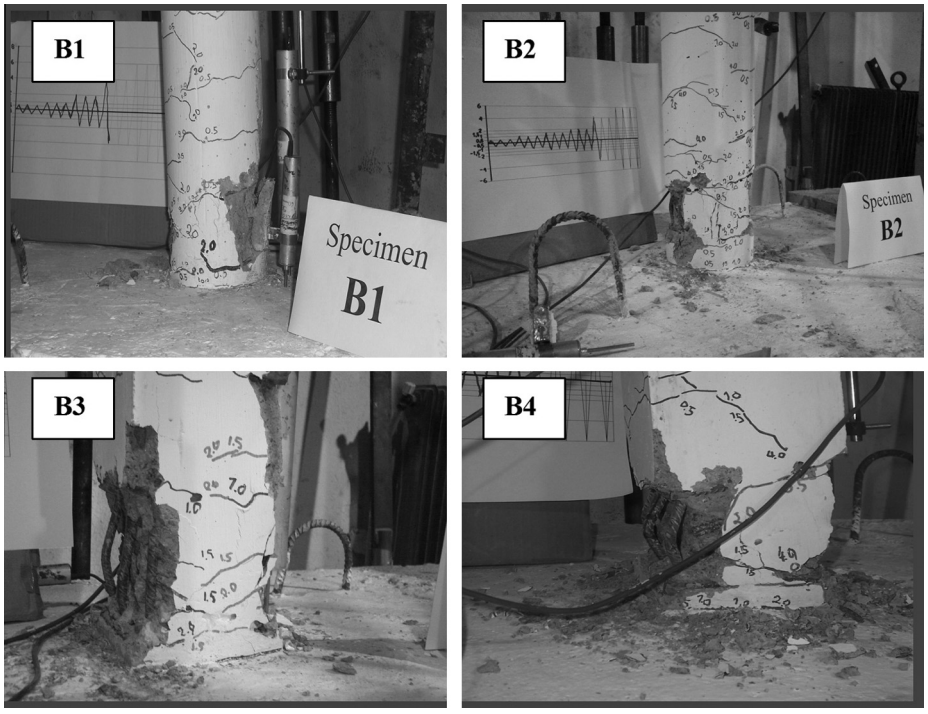

Fig. 13. Failure modes for group B specimens.

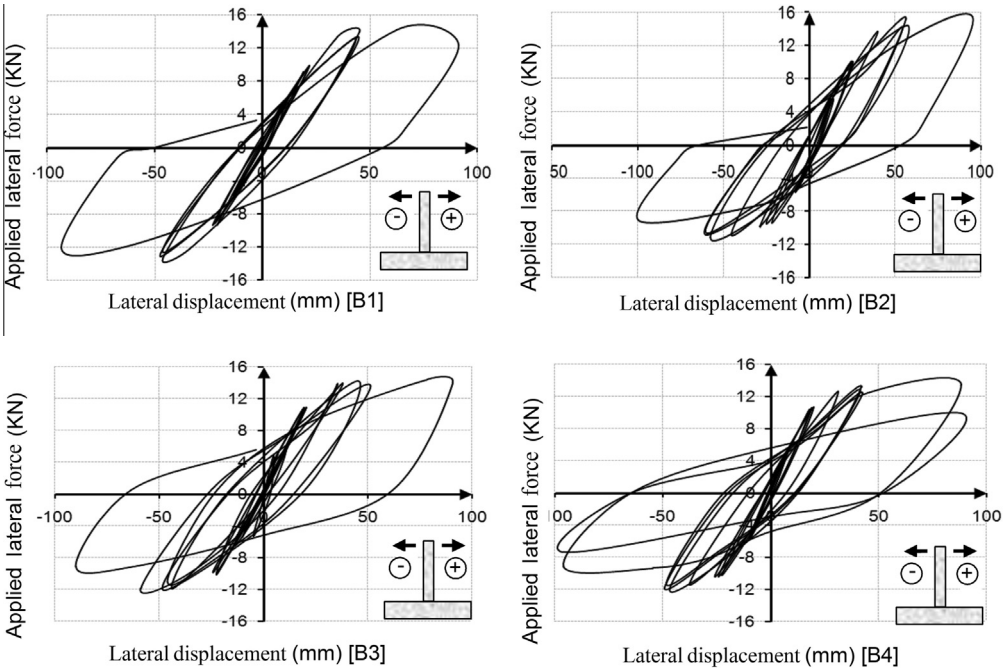

Fig. 14. Cyclic response of column-to-footing joints.

joint region were the same as with A1 and A2, and the cap beam and the joint of A4 were designed with a reduced width, the joint sustained successfully the simulated earthquake loading, while the observed specimen behavior was not significantly compromised as compared with the other two specimens. (Fig. 12). However, contrary to what occurred with a larger joint width, the first minor shear cracks on the joint faces of A4 appeared during the cycle to $0.75F_y$ and continued to propagate for every loading step, forming a dense diagonal cracking net until the end of the test. The joint shear stress at first yielding of the joint (at $1.00F_y$) was estimated equal to $0.42\sqrt{f_{cm}}$ and reached the maximum value of $0.71\sqrt{f_{cm}}$ at maximum applied load. The specimen showed excessive flexural inelasticity in the column (Fig. 12), with spalling of cover concrete at the column critical region during the second cycle at $\mu_\Delta = 4.0$ and buckling of longitudinal column reinforcement at $\mu_\Delta = 6.0$. The test was again terminated due to exhaustion of the actuator travel without a significant loss of strength of the specimen. Slip of the extreme longitudinal column reinforcement at first joint

yielding was estimated about 1.0 mm, but could not be similarly calculated towards the end of the test because of detachment of the critical displacement transducer.

4.5. Connection with a box-girder and through passage in the joint – specimen A5

Specimens A5 and A6 represented pier-superstructure monolithic connections in the longitudinal bridge axis, and therefore the beam had a box section simulating a main girder. Here a longitudinal opening through the joint occurred compromising the continuity of the joint body. The first flexural cracks at the column critical region and the first minor shear cracks at the joint faces were observed already from the first cycle to a load of $0.50F_y$. These cracks propagated during the following cycles to $0.50F_y$, whereas new minor shear cracks appeared along the column. For the loading step to $0.75F_y$ the diagonal shear cracks at the joint faces propagated along the anchorages of the longitudinal column reinforcement, indicating large values of anchorage slip. For the first cycle to $1.00F_y$ the diagonal cracks at the joint faces became 2–3 mm wide and spalling of the concrete cover of the joint reinforcement began, while the column flexural cracks at joint-column interface increased suddenly. Upon reversal of the applied load at the column end the displacement of the specimen was increased abruptly at an almost constant value of the applied force. In the second cycle to $1.00F_y$ the specimen exhibited a shear-type failure (Fig. 12) because of punching of the cap beam along the joint boundaries (Fig. 8). Punching was marked by concrete spalling at the bottom beam face (Fig. 11) along a circumferential crack line, about 10–20 cm away from the perimeter of the connected column. At specimen failure, flexural cracks at the top face of the beam were also observed; the cracks were wider at the location of beam-joint interface. The maximum joint shear stress was recorded at failure (first cycle at $1.00F_y$), equal to $0.78\sqrt{f_{cm}}$, whereas the associated joint distortion was 0.00037 rad. In the second cycle to $1.00F_y$ the joint distortion exceeded the value of 0.001 rad which was the highest value of distortion observed among all specimens at the loading step to $1.00F_y$. The value of anchorage slip of the longitudinal column reinforcement exceeded 20.0 mm in the end of the test; this was also the highest value that was observed among all specimens for the loading step to $1.00F_y$.

4.6. Connection of box-girder with pier – specimen A6

Specimen A6 differed from A5 in that the box girder had rigid end diaphragms and no opening in the monolithic connection with the pier. During the force-controlled cycles of the test, A6 showed flexural cracks in the column critical area without any shear cracks at the joint faces. At the loading steps to ductilites $\mu_\Delta = 1.5$ and 2.0, the flexural cracks in the column critical region propagated, while shear cracks appeared along the column. The first diagonal minor cracks were also observed on the joint faces. The joint shear cracks extended to the bottom beam face until the perimeter of the column taking on a radial direction towards the center of the column section. At $\mu_\Delta = 4.0$, spalling of concrete in the column critical section was observed, whereas the column flexural cracks near the joint–column interface propagated (Fig. 11), indicating large values of anchorage slip of the column longitudinal reinforcement. For the cycle to $\mu_\Delta = 6.0$ the column longitudinal bars buckled and the specimen underwent strength degradation (Fig. 8). Yielding of the joint occurred simultaneously with the column at $\mu_\Delta = 1.0$, with the joint distortion exceeding the value of 0.0002 rad and the joint shear stress reaching the value of $0.35\sqrt{f_{cm}}$. The maximum developed joint shear stress was $0.49\sqrt{f_{cm}}$ in the first cycle up to $\mu_\Delta = 4.0$, while the associated distortion was 0.0007 rad. Another fact that testified joint yielding was the slip value of the column anchorages that was estimated about 1.7 mm for $\mu_\Delta = 1.0$, but reached 20.0 mm in the end of the test. However, the overall behavior of specimen A6 was deemed satisfactory and compliant to the design intentions. The joint of the specimen maintained its capacity, whereas the column of the specimen showed extensive flexural inelasticity in the plastic hinge region (Fig. 12). The test was terminated when the available travel of the actuator was exhausted.

4.7. Pier-foundation control specimen B1

The authors' objective relative to testing group B specimens was to establish if the depth of the joint and the shape of the column (circular vs. square) may affect significantly the behavior of the joint undergoing shear and moment transfer. Through comparisons of specimens B2, B3, and B4 with the control specimen B1, conclusions are drawn with regards the area of the joint that is effectively mobilized in shear action. Flexural cracks in the circular-section column of B1 first appeared during the load cycle to $0.50F_y$ and continued to propagate until the end of the test. In the displacement excursion to $\mu_\Delta = 2.0$ spalling of concrete was observed in the critical column region. The spalling extended and spread up to $\mu_\Delta = 4.0$, when the column reinforcement under compression started to buckle. The test ended in the displacement cycle to $\mu_\Delta = 4.0$ having exhausted the available actuator travel with no loss of strength in the specimen. No cracks were observed at the top or the side footing faces. Yielding of the joint was marked by the slip of column reinforcement which was estimated equal to 2.6 mm at $1.00F_y$; thus displacement was equal to 6.5 mm at $\mu_\Delta = 2.0$ and exceeded 12.00 mm near the end of the test, without a proportional increase in the applied forces. The developed joint shear stress was estimated equal to $0.42\sqrt{f_{cm}}$ at $1.00F_y$ and reached a peak value of $0.61\sqrt{f_{cm}}$ at $\mu_\Delta = 4.0$. The overall behavior of the specimen was excellent with the damage concentrated in the column critical region (Figs. 13 and 14).

4.8. Circular column, reduced connection height – specimen B2

Although specimen B2 was designed with a reduced footing height in comparison with specimen B1, it showed the same excellent behavior as specimen B1 under the same reversed cyclic load history (Fig. 8). The joint yielded at $1.00F_y$, but maintained its capacity until the end of the test where damage was concentrated in the critical region of the column (Figs. 13 and 14). Joint yielding was not externally discernible except for the anchorage slip of the column longitudinal reinforcement that was estimated equal to 3.6 mm at $1.00F_y$, equal to 7.5 mm at $\mu_\Delta = 2.0$ and exceeded 10.0 mm in the end of the test. The developed joint shear stress was estimated equal to $0.57\sqrt{f_{cm}}$ at $1.00F_y$ and reached a peak value of $0.87\sqrt{f_{cm}}$ at $\mu_\Delta = 4.0$. Despite the large values of shear stress, distress in the joint region was not manifested with damage – clearly the foundation plate provided significant confinement that enhanced the available strength, consistent with the guidelines for technical committees such as ACI-ASCE 352 which consider the redundancy of the connection in establishing the magnitude of allowable joint shear stresses [20].

4.9. The effect of square column section – specimen B3

The behavior of specimen B3 was very similar to that of B1. Flexural cracks first appeared in the column at the loading cycle to $0.50F_y$ and continued to propagate until the end of the test. Spalling of concrete occured in the column critical region during the cycle at $\mu_\Delta = 2.0$ and continued to propagate up to $\mu_\Delta = 4.0$, while the column reinforcement under compression started to buckle. The test ended at $\mu_\Delta = 4.0$ because of termination of the

range of the loading ram, while the specimen maintained its capacity. Minor cracks were also observed in the top face of the footing at $\mu_\Delta = 1.5$ indicating the onset of damage inside the joint, however, this type of damage did not extend upon further loading to higher displacements. Yielding of the joint was also testified by the anchorage slip of column reinforcement which was estimated equal to 1.3 mm at $1.00F_y$ and equal to 3.6 mm at $\mu_\Delta = 2.0$ (slip could not be measured at $\mu_\Delta = 4.0$ because of detachment of the critical DT). The developed joint shear stress was estimated equal to $0.50\sqrt{f_{cm}}$ at $1.00F_y$ and reached a peak value of $0.66\sqrt{f_{cm}}$ at $\mu_\Delta = 4.0$; these values are comparable to those recorded at similar displacement ductility levels in B1, justifying the assumption of an equal effective joint area in the two cases. The overall behavior of the specimen was excellent with the damage concentrated in the column critical region (Figs. 13 and 14).

4.10. Rectangular column, reduced connection height – specimen B4

Although specimen B4 was designed with a reduced footing height in comparison with specimen B3, it showed the same excellent behavior as B3 under the reversed cyclic loads (Fig. 8). The joint yielded at $1.00F_y$, but it maintained its capacity until the end of the test where the damage was concentrated in the critical region of the column. Joint yielding was externally observed by minor cracks that appeared on the top face of the footing at $\mu_\Delta = 1.5$ and by the anchorage slip of the column longitudinal reinforcement which was estimated equal to 1.1 mm at $1.00F_y$, and increased to 3.6 mm at $\mu_\Delta = 2.0$ exceeding to 8.0 mm near the end of the test. The developed joint shear stress was estimated equal to $0.63\sqrt{f_{cm}}$ at $1.00F_y$ and reached a peak value of $0.80\sqrt{f_{cm}}$ at $\mu_\Delta = 4.0$. Again, as in the case of specimen B2, joint shear stresses are well above what is considered allowable for T-type connections (see ACI-ASCE 352 [20]), confirming that the footing slab surrounding the connection provides significant confinement that eventually suppresses joint shear damage and degradation.

4.11. Discussion of the overall behavior traits of the specimens

All specimens that represented monolithic T-connections in the direction perpendicular to bridge axis (A1–A4) showed satisfactory behavior under simulated earthquake loading, with flexural inelastic deformations and damage prevailing in the column critical area. Specimens A1, A2 and A4 behaved as intended by the modern bridge design standards (yielding of the column, no joint failure), developing a network of minor shear cracks at advanced stages of loading. The shear cracking net was denser in the case of A4 specimen which was designed with a reduced cap beam width, nevertheless without affecting its overall behavior. Assessment of the joint region of specimen A3 with an opening through the joint was shown to be much better than expected. Although wide diagonal shear cracks and concrete spalling were observed on the joint faces of A3, the joint sustained successfully the applied cyclic loading whereas the specimen failed by excessive column flexural yielding. The satisfactory behavior of A1–A4 specimens (especially this of A3) is attributed to the good anchorage conditions of the longitudinal column bars that were supplied with a hook in the end of their anchorage.

Specimens that represented T-joints in the direction along the bridge axis (A5 and A6) showed a different behavior under reversed cyclic loading. Specimen A5 with the passage-opening in the joint body developed shear-type failure because of punching of the cap beam along the joint boundaries. On the contrary, the behavior of A6 was deemed satisfactory marked by wide hysteresis loops and characteristic inelastic flexural damage in the column critical area. Thus, construction of openings for inspection passage within the joint body is deemed deprecating to the joint and should be discouraged. The direction parallel to the bridge axis is considered to be critical for these connections as it eradicates the center of the panel where the diagonal compression strut forms in the joint enabling shear transfer (ACI 352R-02 [20]).

All group B specimens showed excellent seismic behavior with the damage concentrated in the column critical area because of extensive column flexural yielding. Few minor cracks were observed only on the upper face of the footings for the specimens with rectangular column section (B3 and B4). However, the type of column section (circular or rectangular) did not affect the overall specimen behavior, with all specimens developing wide hysteresis loops and increased energy absorption. The satisfactory behavior of group B specimens is attributed to the good anchorage conditions of the longitudinal column bars that were supplied with a 90° hook in the end of their anchorage towards the interior of the joints. Joint shear strains of the specimens that were calculated from measurements on footing faces were deemed inaccurate with reference to estimating joint distortion and were not used further due to the large distance of the footing faces from the joint center. The magnitudes of joint shear stresses in the specimens with the reduced connection depth were well within the limits also prescribed by the ACI-ASCE technical committee for T-joints ($1.25\sqrt{f_{cm}}$ and $1\sqrt{f_{cm}}$ for three vertical faces and two vertical faces of the joint being confined). The difference in performance between the A and the B group of specimens also underscores the confining influence of the footing slab which precludes the occurrence of joint failure at the expense of greater damage in the column plastic hinge region at advanced levels of lateral displacement; this effect is accounted for explicitly through coefficient α_c in the EC8-II [1] provisions (see Eq. (A.10) in the Appendix).

5. Conclusions

The experimental study demonstrated that design and detailing of pier-superstructure monolithic connections according with the EC8-II [1] leads to a satisfactory performance under earthquake loading. Based on the observed response it was concluded that special care ought to be provided for the design of the anchorages of the pier longitudinal reinforcement according with EC2 [19], in order to prevent joint failure due to anchorage pullout. Placing a fraction of the necessary vertical joint reinforcement in the beams outside the joint, as suggested in EC8-II [1] for congestion-free alternative detailing did not compromise the strength of the joint, whereas this practice facilitates placement of the reinforcement during construction. In all cases discontinuities in the joint body such as openings for passage ought to be avoided.

Generally, design and detailing of monolithic connections between pier and caissons according with EC8-II [1] and EC2 [19] (for detailing of anchorages) leads to very good connection performance under earthquake loading. The minimum footing height required by the code is shown to be conservative, as the specimens with a reduced footing height (B2 and B4) behaved also excellently. More experimental and analytical work should be carried out on this aspect with particular emphasis on larger specimen sizes before lowering the code requirements with regards the minimum required footing height, with a commensurate saving in the amounts of concrete and reinforcing steel used in construction.

Using the code specified dimensions for the joint region, shear stresses sustained by the joint ranged between $0.29\sqrt{f_{cm}}$ to $0.7\sqrt{f_{cm}}$ at first yielding of the joint, and between $0.45\sqrt{f_{cm}}$ and $0.98\sqrt{f_{cm}}$ in the ultimate state. This disparity suggests that the provisions defining joint boundaries may admit refinement, to estimate similar levels of stress at milestone events in the joint, while the stress limits are properly linked explicitly to the amount of confinement available in the connection in the EC8-II [1] provisions.

Acknowledgements

The work presented in the paper was funded by the Greek General Secretariat for Research and Technology through the project "Seismic Protection of Bridges". The second author would like to thank also the Alexander S. Onassis Public Benefit Foundation whose financial support is greatly appreciated.

Appendix A. Background to joint design provisions in EC8-II [1]

For verification of the joint, the average nominal shear stresses are defined as follows:

(a) Joint shear stress:

$$v_j = v_{jx} = v_{jz} = \frac{V_{jx}}{b_{j,eff}\cdot z_c} = \frac{V_{jz}}{b_{j,eff}\cdot z_b} \tag{A.1}$$

(b) Joint axial stresses:

$$n_z = \frac{N_{jz}}{b_{j,eff}\cdot h_c}, \quad n_x = \frac{N_{jx}}{b_{j,eff}\cdot h_b}, \quad n_y = \frac{N_{jy}}{b_{j,eff}\cdot h_c} \tag{A.2}$$

Joint verification checks are used to determine the required joint reinforcement (in the form of closed stirrups arranged in the horizontal and the vertical direction in the body of the joint) from equilibrium considerations: the total force that the stirrups may develop in each direction should exceed the tensile stress resultant that may be supported by the joint concrete volume prior to cracking in the direction considered (uniform stress distribution is assumed in each section through the joint):

$$\begin{aligned} F_{sy,x} &= f_{ctd}\cdot b_{j,eff}\cdot h_b \;\Rightarrow f_{sy,x}\cdot A_{sx} = f_{ctd}\cdot b_{j,eff}\cdot h_b \;\Rightarrow \frac{A_{sx}}{b_{j,eff}\cdot h_b} \\ &= \frac{f_{ctd}}{f_{sy,x}} \;\Rightarrow \rho_{x,\min} = \frac{f_{ctd}}{f_{sy,x}} \end{aligned} \tag{A.3}$$

$$\begin{aligned} F_{sy,z} &= f_{ctd}\cdot b_{j,eff}\cdot h_c \;\Rightarrow f_{sy,z}\cdot A_{sz} = f_{ctd}\cdot b_{j,eff}\cdot h_c \;\Rightarrow \frac{A_{sz}}{b_{j,eff}\cdot h_c} \\ &= \frac{f_{ctd}}{f_{sy,z}} \;\Rightarrow \rho_{z,\min} = \frac{f_{ctd}}{f_{sy,z}} \end{aligned} \tag{A.4}$$

where $f_{ctd} = f_{ctk0.05}/\gamma_c$ the design tensile strength of concrete, $f_{sy,x}$ and $f_{sy,z}$ are the yielding strength values of joint shear reinforcement in directions x and z respectively and A_{sx}, A_{sz} are the areas of joint shear reinforcement in the form of closed stirrups in directions x and z respectively.

The joint shear reinforcement ratios in each direction ($\rho_{x,\max}$ and $\rho_{z,\max}$) may not exceed the result of Eqs. (A.5) and (A.6) below which is related to the horizontal force resultant in the direction considered, at crushing of the diagonal compressive strut in the joint.

$$\begin{aligned} F_{sy,x} &= 0.5\cdot\nu\cdot f_{cd}\cdot b_{j,eff}\cdot h_b \;\Rightarrow\; f_{sy,x}\cdot A_{sx} \\ &= 0.5\cdot\nu\cdot f_{cd}\cdot b_{j,eff}\cdot h_b \;\Rightarrow \frac{A_{sx}}{b_{j,eff}\cdot h_b} = \frac{0.5\cdot\nu\cdot f_{cd}}{f_{sy,x}} \\ &\Rightarrow\; \rho_{x,\max} = \frac{0.5\cdot\nu\cdot f_{cd}}{f_{sy,x}} \end{aligned} \tag{A.5}$$

$$\begin{aligned} F_{sy,z} &= 0.5\cdot\nu\cdot f_{cd}\cdot b_{j,eff}\cdot h_c \;\Rightarrow\; f_{sy,z}\cdot A_{sz} \\ &= 0.5\cdot\nu\cdot f_{cd}\cdot b_{j,eff}\cdot h_c \;\Rightarrow \frac{A_{sz}}{b_{j,eff}\cdot h_c} = \frac{0.5\cdot\nu\cdot f_{cd}}{f_{sy,z}} \\ &\Rightarrow\; \rho_{z,\max} = \frac{0.5\cdot\nu\cdot f_{cd}}{f_{sy,z}} \end{aligned} \tag{A.6}$$

where f_{cd} the design cylinder compressive strength of concrete, and $\nu = 0.60\cdot(1-(f_{ck}/250))$ with f_{ck} (in MPa) the coefficient of reduction of the compressive strength of concrete due to the presence of transverse tensile strains.

The joint is assumed to have developed diagonal cracking (EC8-II [1]), when the principal tensile stress of concrete exceeds the tensile strength of the joint. Therefore, shear cracking stress of the joint $v_{j,cr}$ can be evaluated if the principal tensile stress of concrete is set equal to the design tensile stress f_{ctd} of concrete (sign-convention is tension-positive):

$$\begin{aligned} \sigma_1 &= \frac{n_x+n_z}{2} + \sqrt{\left(\frac{n_x-n_z}{2}\right)^2 + v_{jz}^2} \;\Rightarrow\; f_{ctd} \\ &= \frac{n_x+n_z}{2} + \sqrt{\left(\frac{n_x-n_z}{2}\right)^2 + v_{j,cr}^2} \;\Rightarrow\; v_{j,cr}^2 \\ &= (f_{ctd}-n_x)\cdot(f_{ctd}-n_z) \;\Rightarrow\; v_{j,cr} \\ &= f_{ctd}\cdot\sqrt{\left(1-\frac{n_x}{f_{ctd}}\right)\cdot\left(1-\frac{n_z}{f_{ctd}}\right)} \end{aligned} \tag{A.7}$$

The design expression (EC8-II [1]) is obtained from Eq. (A.7) by replacing the axial compressive stresses with the absolute values (provided that forces are compressive):

$$v_{j,cr} = f_{ctd}\cdot\sqrt{\left(1+\frac{n_x}{f_{ctd}}\right)\cdot\left(1+\frac{n_z}{f_{ctd}}\right)} \tag{A.8}$$

In order to use minimum transverse reinforcement in the joint region it is required that the average shear stress of the joint v_j does not exceed the cracking shear capacity of the joint $v_{j,cr}$ (from Eqs. (A.3) and (A.4)):

$$v_j \leqslant v_{j,cr} = f_{ctd}\cdot\sqrt{\left(1+\frac{n_x}{f_{ctd}}\right)\cdot\left(1+\frac{n_z}{f_{ctd}}\right)} \leqslant 1.50\cdot f_{ctd} \tag{A.9}$$

If the shear stress demand in the joint exceeds the cracking shear capacity, then it is required that it does not exceed the shear failure stress of the joint. With reference to failure by crushing of the diagonal compressive strut that forms in the joint body (ACI 352R-02 [21]), the shear strength of concrete is taken equal to the half of its compressive strength; the compressive strength is determined by taking into account not only the presence of transverse tensile strains (through coefficient ν) but also the effect of confinement in the transverse direction y (through coefficient α_c). Therefore:

$$v_j \leqslant v_{j,Rd} = 0.50\cdot\alpha_c\cdot\nu\cdot f_{cd} \quad \text{(in MPa)} \tag{A.10}$$

where ν is as defined in Eq. (A.6), $\alpha_c = 1 + 2(n_{jy} + \rho_y f_{sd})/f_{cd} \leqslant 1.50$ accounts for the strength enhancement of the diagonal compressive strut imparted by confining stress n_{jy} (if present) and/or the percentage of closed stirrup reinforcement ρ_y in the transverse direction y (orthogonal to the plane of action), defined by $\rho_y = A_{sy}/(h_c\cdot h_b)$. To control the extent of joint cracking, transverse reinforcement stress is limited to $f_{sd} = 300$ MPa.

In the general design case where $v_{j,cr} \leqslant v_j \leqslant v_{j,Rd}$ the necessary amounts of joint shear reinforcement ρ_x and ρ_z to be placed in horizontal and vertical directions respectively, are defined from equilibrium of the forces in each direction:

$$\begin{aligned} \sigma_x &= -\rho_x\cdot f_x - n_x \Rightarrow -v_j\cdot\tan\theta = -\rho_x\cdot f_{xy} - n_x \overset{\theta\approx 45^o}{\Rightarrow} \rho_x \\ &= \frac{v_j-n_x}{f_{xy}} \Rightarrow \frac{A_{sx}}{b_{j,eff}\cdot h_b} = \frac{v_j-n_x}{f_{xy}} \end{aligned} \tag{A.11}$$

$$\begin{aligned} \sigma_z &= -\rho_z\cdot f_z - n_z \Rightarrow -\frac{v_j}{\tan\theta} = -\rho_z\cdot f_{zy} - n_z \overset{\theta\approx 45^o}{\Rightarrow} \rho_z \\ &= \frac{v_j-n_z}{f_{zy}} \Rightarrow \frac{A_{sz}}{b_{j,eff}\cdot h_c} = \frac{v_j-n_z}{f_{zy}} \end{aligned} \tag{A.12}$$

The following Appendices present examples of calculation of specimen details according to the EC8-II provisions summarized herein (one pier-superstructure and one pier-foundation case).

Appendix B

The reinforcement of specimen A1 (pier to cap-beam connection) was determined according to the design provisions of EC8-II [1].

– Effective width of the joint:

$$b_j = \min\{b_w,\ b_c + 0.5 \cdot h_c\} \overset{\substack{b_c = 0.9 \cdot d_c \\ h_c = 0.9 \cdot d_c}}{\Rightarrow} b_j = \min\{0.54,\ 1.35 \cdot 0.35\}$$

$$\Rightarrow \quad b_j = 473 \text{ mm}$$

– Forces transferred through the joint:

$$V_{jz} = \gamma_o \cdot T_{Rc} - V_{1bC} = \gamma_o \cdot 0.5 \cdot A_{sc} \cdot f_y - V_{1bC} \Rightarrow V_{jz} = 1.35 \cdot 0.5 \cdot 14 \cdot 1.13 \cdot 10^{-4} \cdot 500 + 0.0604 = 0.474 \text{ MN}$$

$$N_{jz} = 0.5 \cdot N_{cG} \cdot \frac{A_c}{A_{j.eff}} = 0.5 \cdot N_{cG} \cdot \frac{b_c}{b_j} = 0.5 \cdot 0.050 \cdot \frac{0.9 \cdot 0.35}{0.473} = 0.017MN$$

– Joint stresses: $v_j = v_{jv} = \frac{V_{jz}}{b_j \cdot z_b} = \frac{0.474}{0.473 \cdot 0.9 \cdot 0.40} = 2.78$ MPa

$$n_z = \frac{N_{jz}}{b_j \cdot h_c} = \frac{0.017}{0.473 \cdot 0.9 \cdot 0.35} = 0.114 \text{ MPa}$$

– Joint shear stress at cracking:

$$v_{j,cr} = f_{ctd} \cdot \sqrt{\left(1 + \frac{n_z}{f_{ctd}}\right)} = \frac{1.80}{1.5} \cdot \sqrt{\left(1 + \frac{0.114}{1.80/1.5}\right)} = 1.26 \text{ MPa} \leqslant 1.50 \cdot f_{ctd}$$

– $v_j \geqslant v_{j,cr}$, thus shear reinforcement is required. Check that $v_j \leqslant v_{j,Rd} = 0.50 \cdot \alpha_c \cdot \nu \cdot f_{cd}$ ($\alpha_c = 1$ conservatively neglecting the strength enhancement due to confinement):

$$v_{j,Rd} = 0.50 \cdot \left[0.60 \cdot \left(1 - \frac{25}{250}\right)\right] \cdot \frac{25}{1.5} = 4.50 \text{ MPa} > 2.78 \text{ MPa} = v_j$$

– Required ratios of joint shear reinforcement:
– Horizontal ρ_x

$$\rho_x = \frac{v_j}{f_{sy}} = \frac{A_{sx}}{b_j \cdot h_b} \rightarrow \begin{cases} \geqslant \rho_{\min} = \frac{f_{ctd}}{f_{sy}} = \frac{1.8/1.5}{500/1.15} = 0.00276 \\ \leqslant \rho_{\max} = \frac{0.5 \cdot \nu \cdot f_{cd}}{f_{sy}} = \frac{0.5 \cdot 0.6 \cdot [1 - (25/250)] \cdot 25/1.5}{500/1.15} = 0.01035 \end{cases}$$

$$\rho_x = \frac{2.78}{500/1.15} = 0.00639 = \frac{A_{sx}}{0.473 \cdot 0.40} \ \Rightarrow \ A_{sx} = 1210 \ \text{mm}^2$$

Available beam reinforcement: $(6\Phi14 + 4\Phi12)/2 = 686$ mm^2. Available from column spiral: $(0.35/0.05) \cdot 2 \ \Phi10 = 1099$ mm^2. Total: 1785 mm^2, suffices (no additional reinf. is needed).

– Vertical ρ_z

$$\rho_z = \frac{v_j - n_z}{f_{sy}} = \frac{A_{sz}}{b_j \cdot h_c} \rightarrow \begin{cases} \geqslant \rho_{\min} = \frac{f_{ctd}}{f_{sy}} = 0.00276 \\ \leqslant \rho_{\max} = \frac{0.5 \cdot \nu \cdot f_{cd}}{f_{sy}} = 0.01035 \end{cases}$$

$$\rho_z = \frac{2.78 - 0.114}{500/1.15} = 0.00613 = \frac{A_{sz}}{0.473 \cdot 0.9 \cdot 0.35} \ \Rightarrow \ A_{sz} = 914 \text{ mm}^2$$

– Required vertical shear reinforcement: 5 layers of four-leg $\Phi8$ (1006 mm^2).

Appendix C

This section summarizes application of the Code provisions for calculation of required reinforcement for specimen B1:

– Effective joint width:

$$b_j = \min\{b_w,\ b_c + 0.5 \cdot h_c\} \overset{\substack{b_c = 0.9 \cdot d_c \\ h_c = 0.9 \cdot d_c}}{\Rightarrow} b_j = \min\{0.80,\ 1.35 \cdot 0.15\}$$

$$\Rightarrow \quad b_j = 200 \text{ mm}$$

– Joint stresses:

$$V_{jz} = \gamma_o \cdot T_{Rc} - V_{1bC} = \gamma_o \cdot 0.5 \cdot A_{sc} \cdot f_y - V_{1bC} \Rightarrow V_{jz} = 1.35 \cdot 0.5 \cdot 6 \cdot 0.50 \cdot 10^{-4} \cdot 500 + 0.00 = 0.100MN$$

$$v_j = v_{jv} = \frac{V_{jz}}{b_j \cdot z_b} = \frac{0.100}{0.20 \cdot 0.9 \cdot 0.20} = 2.78 \text{ MPa}$$

$$N_{jz} = 0.5 \cdot N_{cG} \cdot \frac{A_c}{A_{j.eff}} = 0.5 \cdot 0.050 \cdot \frac{0.9 \cdot 0.15}{0.20} = 0.017MN;$$

$$n_z = \frac{N_{jz}}{b_j \cdot h_c} = \frac{0.017}{0.20 \cdot 0.9 \cdot 0.15} = 0.63 \text{ MPa}$$

– Joint shear cracking stress:

$$v_{j,cr} = f_{ctd} \cdot \sqrt{\left(1 + \frac{n_z}{f_{ctd}}\right)} = \frac{1.80}{1.5} \cdot \sqrt{\left(1 + \frac{0.63}{1.80/1.5}\right)} = 1.48 \text{ MPa} \leqslant 1.50 \cdot f_{ctd}$$

Since $v_j \geqslant v_{j,cr}$ shear reinforcement in the joint is required. Check that $v_j \leqslant v_{j,Rd} = 0.50 \cdot \alpha_c \cdot \nu \cdot f_{cd}$ with $\alpha_c = 1$ (for conservatism):

$$v_{j,Rd} = 0.50 \cdot \left[0.60 \cdot \left(1 - \frac{25}{250}\right)\right] \cdot \frac{25}{1.5} = 4.50 \text{ MPa} > 2.78 \text{ MPa} = v_j$$

– Required ratios of joint shear reinforcement.
– Horizontal, ρ_x:

$$\rho_x = \frac{v_j}{f_{sy}} = \frac{A_{sx}}{b_j \cdot h_b} \rightarrow \begin{cases} \geqslant \rho_{\min} = \frac{f_{ctd}}{f_{sy}} = \frac{1.8/1.5}{500/1.15} = 0.00276 \\ \leqslant \rho_{\max} = \frac{0.5 \cdot \nu \cdot f_{cd}}{f_{sy}} = \frac{0.5 \cdot 0.6 \cdot [1 - (25/250)] \cdot 25/1.5}{500/1.15} = 0.01035 \end{cases}$$

$$\rho_x = \frac{2.78}{500/1.15} = 0.00639 = \frac{A_{sx}}{0.20 \cdot 0.20} \ \Rightarrow \ A_{sx} = 256 \text{ mm}^2$$

– Available reinforcement in the effective width of the joint: Beam reinforcement: $(2\Phi8)/2 = 50$ mm^2; continuation of column spiral reinforcement in the joint $(0.20/0.10) \cdot 2\Phi6 = 112$ mm^2. Total available: 162 mm^2. Required additional hoops: two layers $\Phi6$ (113 mm^2).
– Vertical ρ_z:

$$\rho_z = \frac{v_j - n_z}{f_{sy}} = \frac{A_{sz}}{b_j \cdot h_c} \rightarrow \begin{cases} \geqslant \rho_{\min} = 0.00276 \\ \leqslant \rho_{\max} = 0.01035 \end{cases}$$

$$\rho_z = \frac{2.78 - 0.63}{500/1.15} = 0.0049 = \frac{A_{sz}}{0.20 \cdot 0.9 \cdot 0.15} \ \Rightarrow \ A_{sz} = 132 \text{mm}^2$$

Vertical shear reinforcement placed inside the joint: 2 inverted U shapes, $\Phi6$ (113 mm^2).

References

[1] Eurocode 8 (EC-8). Design of structures for earthquake resistance – Part 2 (II): Bridges. CEN, Brussels: European Committee for Standardization; 2005.
[2] Priestley MJN, Seible F. Assessment of bridge damage during the loma prieta earthquake. University of California San Diego, Structural Systems Research Project. Report No. SSRP-90/01; 1990.
[3] Thewalt CR, Stojadinovic B. Behavior of bridge outrigger knee joint systems. EERI Earthquake Spectra 1995;11(3):477–508.

[4] Xiao Y, Priestley MJN, Seible F. Seismic assessment and retrofit of bridge column footings. ACI Struct J 1996;93(1):79–94.
[5] Sexsmith R, Anderson D, English D. Cyclic behavior of concrete bridge bents. ACI Struct J 1997;94(2):103–14.
[6] Priestley MJN, Seible F, MacRae GA, Chai YH. Seismic assessment of the santa monica viaduct bent. ACI Struct J 1997;94(5):513–24.
[7] Ingham JM, Priestley MJN, Seible F. Cyclic response of bridge knee joints with circular columns. ICP J Earthq Eng 1998;2(3):357–90.
[8] Lowes LN, Moehle JP. Evaluation of retrofit of beam-column T-joints in older reinforced concrete bridge structures. ACI Struct J 1999;96(4):519–33.
[9] McLean D, Marsh M. Seismic retrofitting of bridge foundation. ACI Struct J 1999;99(2):174–83.
[10] Mazzoni S, Moehle JP. Seismic response of beam-column joints in double deck reinforced concrete bridge frames. ACI Struct J 2001;98(3):259–69.
[11] Sritharan S, Priestley MJN, Seible F. Seismic design and experimental verification of concrete multiple column bridge bents. ACI Struct J 2001;98 (3):335–46.
[12] Naito CJ, Moehle JP, Mosalam KM. Experimental and computation evaluation of reinforced concrete bridge beam-column connections for seismic performance. PEERC Report 2001;08:1–232.
[13] Pantelides C, Gergely J, Reaveley L. In-situ verification of rehabilitation & repair of R/C bridge bents under simulated seismic loads. EERI Earthq Spectra 2001;17(3):507–30.
[14] Gibson N, Filiatrault A, Ashford SA. Performance of beam to column bridge joints subjected to a large velocity pulse. PEERC Report 2002;24:1–87.
[15] California Transportation Agency. Caltrans seismic design criteria Ver. 3.1.; 2004.
[16] Timosidis D, Pantazopoulou SJ. Anchorage of longitudinal column reinforcement in bridge monolithic connections. ASCE J Struct Eng 2009;135 (4):344–55.
[17] Egnatia Odos AE. Categories of representative bridges of Egnatia highway based on their structural characteristics: electronic file in Greek.
[18] Timosidis D. Design and seismic behaviour of monolithic connections in reinforced concrete structures – emphasis in reinforced concrete bridges. PhD dissertation. Greece: Department of Civil Engineering, Demokritus University of Thrace, Xanthi [in Greek].
[19] Eurocode 2 (EC-2). Design of concrete structures – Part 2: Concrete bridges. Design and detailing rules. CEN, Brussels: European Committee for Standardization; 2005.
[20] ACI 352R-02. Recommendations for beam column connections in monolithic reinforced concrete structures. In: Technical committee ACI-ASCE 352. Farmington Hills, USA: ACI; 2010.